

## Electronic Supplementary Information

### Highly Emissive Hybrid Mesoporous Organometallo-Silica Nanoparticles for Bioimaging

Cintia Ezquerro,<sup>a</sup> Iciar P. López,<sup>b</sup> Elena Serrano,<sup>c</sup> Elvira Alfaro-Arnedo,<sup>b</sup> Elena Lalinde,<sup>a</sup> Ignacio M. Larráyoza,<sup>\*d,e</sup> José G. Pichel,<sup>b,f</sup> Javier García-Martínez<sup>\*c</sup> Jesús R. Berenguer<sup>\*a</sup>

<sup>a</sup> Departamento de Química-Centro de Investigación en Síntesis Química (CISQ), Universidad de La Rioja, Madre de Dios 53, E-26006, Logroño, Spain. <https://investigacion.unirioja.es/grupos/24/detalle>

<sup>b</sup> Unidad de Cáncer de Pulmón y Enfermedades Respiratorias, and <sup>d</sup> Unidad de *Biomarcadores y Señalización Molecular*. Centro de Investigación Biomédica de La Rioja (CIBIR), Fundación Rioja Salud, 26006, Logroño, Spain. [www.cibir.es](http://www.cibir.es)

<sup>c</sup> Laboratorio de Nanotecnología Molecular. Departamento de Química Inorgánica. Universidad de Alicante. Carretera San Vicente s/n, E-03690, Alicante, Spain. [www.nanomol.es](http://www.nanomol.es)

<sup>e</sup> GRUPAC, Unidad Predepartamental de Enfermería, Universidad de La Rioja, Duquesa de la Victoria 88, E-26006, Logroño, La Rioja, Spain.

<sup>f</sup> Spanish Biomedical Research Networking Centre in Respiratory Diseases (CIBERES), ISCIII, E-28029, Madrid, Spain. <https://www.ciberes.org>

## General Methods

Complex  $[\text{Ir}(\text{dfppy})_2(\text{dasipy})]\text{PF}_6$  (**1**) has been characterized by elemental analyses, mass spectrometry and the usual spectroscopic means (Ir, Vis/UV, multinuclear NMR). All the reactions to synthesize complex **1** were performed under Argon atmosphere and anhydrous conditions. Both the precursors ( $[\text{Ir}(\text{dfppy})_2(\mu\text{-Cl})]_2$ ;  $[\text{Ir}(\text{dfppy})_2(\text{NCMe})_2]\text{PF}_6$ ;  $\text{dfppy} = 2\text{-}(2,4)\text{-difluorophenyl-pyridinyl}$ )<sup>1</sup> and the organic ligand (N,N'-dipropyltriethoxysilane-2,2'-bipyridine-4,4'-dicarboxamide, *dasipy*)<sup>2</sup> were synthesized as previously reported. The other reagents were obtained from commercial sources and used without further purification.

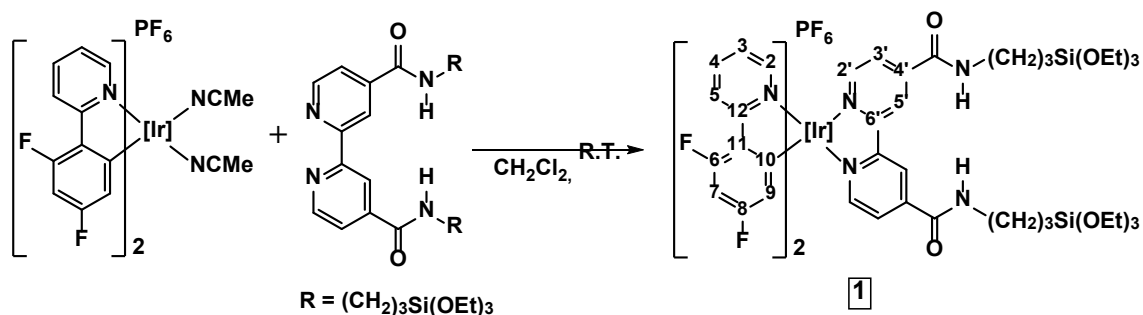
IR spectra were recorded on a Nicolet Nexus FT-IR Spectrometer in the wavenumber range from 4000 to 200  $\text{cm}^{-1}$ . All samples were prepared as KBr pellets. Elemental analyses were carried out in a Perkin-Elmer 2400 CHNS/O and a Thermo Finnigan Flash 1112 microanalyzer. Mass spectra were recorded on a Microflex MALDI-TOF Bruker spectrometer. NMR spectra were recorded on Bruker ARX300 and ARX400 spectrometers. Chemical shifts are reported in parts per million (ppm) relative to external standards ( $\text{SiMe}_4$  for  $^1\text{H}$  and  $^{13}\text{C}\{^1\text{H}\}$ <sup>3</sup> and  $\text{CFCl}_3$  for  $^{19}\text{F}\{^1\text{H}\}$ ) and coupling constants in Hz.  $^1\text{H}$  and  $^{13}\text{C}\{^1\text{H}\}$  NMR spectra were assigned following the numbering scheme indicated in Scheme S1, by means of 2D experiments ( $^1\text{H}\text{-}^1\text{H}$  COSY and  $^1\text{H}\text{-}^{13}\text{C}$  HSQC and HMBC). UV-Vis spectra in solution were recorded on an Agilent 8453 spectrophotometer. Diffuse Reflectance UV-vis (DRUV) spectra were carried out in KBr pellets, using a Shimadzu UV-3600 spectrophotometer with a Harrick praying mantis accessory, and recalculated following the Kubelka Munk function. The excitation and emission spectra were obtained on a Jobin-Yvon Horiba Fluorolog 3-11 Tau-3 spectrofluorimeter. The lifetime measurements were performed operating in the phosphorimeter mode (with a F1-1029 lifetime emission PMT assembly, using a 450 W Xe lamp) or with a Data-Station HUB-B with a nanoLED controller and software DAS6. The nano-LEDs employed for lifetime measurements were of wavelength 370 nm with pulse lengths of 0.8–1.4 ns. The lifetime data were fitted using the Jobin-Yvon software package. Quantum yields were measured using a F-3018 Integrating Sphere mounted on the Fluorolog 3-11 Tau-3 spectrofluorimeter.

For a successful characterization of all the organometallo-silica materials, the NPs suspensions were previously centrifuged and air dried at room temperature. The incorporation of the cyclometalated complex **1** into silica nanoparticles was evaluated by DRUV and FTIR spectroscopic techniques, and the metal contents was determined by

high resolution inductively coupled plasma mass spectrometry (HR-ICP-MS, ELEMENT XR). The samples were dissolved in a mixture of 3,5 mL HCl + 1 mL HNO<sub>3</sub> + 1 mL HF + 5mL H<sub>3</sub>BO<sub>3</sub> (5%), digested in a microwave (260°C, 45 bar) and filtered off (0.45 μm) prior to analysis. This treatment is able to entirely dissolve the samples.

To determine the evolution of the size and surface charge of nanoparticles by dynamic light scattering (DLS) and zeta (ζ) potential measurements, respectively, a Zetasizer Nano ZS (Malvern Instruments, United Kingdom) equipped with a 633 nm “red” laser was used. DLS and ζ potential measurements were directly recorded in aqueous colloidal suspensions. For this purpose, 1 mg of nanoparticles was added to 10 mL of H<sub>2</sub>O Milli-Q, followed by sonication for 15 min to obtain a homogeneous suspension. In both cases, measurements were recorded by placing 1 mL of the suspension (0.1 mg/mL) in DTS1070 disposable folded capillary cells (Malvern Instruments)

The morphology of the mesoporous materials was investigated by transmission electron microscopy (TEM) and scanning electron microscopy (SEM). Samples were prepared by dipping a sonicated suspension of the sample in ethanol on a carbon-coated copper. TEM images were performed using a JEM-2010 microscope (JEOL, 0.14 nm of resolution), at an accelerating voltage of 200 kV. The digital analysis of the TEM micrographs was performed using DigitalMicrograph™ 3.6.1. by Gatan. SEM analyses were carried out in a field emission scanning electron microscope (FESEM) Merlin VP Compact (Zeiss, 1.6 nm of resolution at 1 kV). Porous texture was characterized by nitrogen sorption measurements at 77 K in an AUTOSORB-6 apparatus. The samples were previously degassed at 373 K for 8 h and  $5 \times 10^{-5}$  bars. Adsorption data were analyzed using the software QuadraWin™ (version 6.0) of Quantachrome Instruments. The BET surface area was estimated by using multipoint BET method, using the adsorption data in the relative pressure (P/P<sub>0</sub>) range of 0.05–0.30. Cumulative pore volumes and pore-size distribution curves were calculated using the DFT method (NLDFT adsorption branch model, which assumes nitrogen adsorption at 77 K in cylindrical silica pores for the mesopore range). The total pore volume and the mesopore volume were read directly from the adsorption branch of the isotherm at 0.99 and 0.8, respectively (the micropore volume was determined by using *t*-plot method to be 0).



**Scheme S1.** Synthesis of complex **1**, showing the numbering scheme used in the NMR characterization.

### Synthetic Methods

**Synthesis of [Ir(dfppy)<sub>2</sub>(dasipy)]PF<sub>6</sub> (**1**).** The addition of 0.16 g (0.25 mmol) of *dasipy* in a solution of 0.20 g (0.25 mmol) of [Ir(dfppy)<sub>2</sub>(CH<sub>3</sub>CN)<sub>2</sub>]PF<sub>6</sub> in 30 mL of CH<sub>2</sub>Cl<sub>2</sub> resulted on a yellow mixture that was stirred for 6 hours at room temperature. The resulting solution was evaporated to dryness and the yellow powdery solid was kept under inert conditions to avoid the condensation of the solid (0.27 g, 81%). Anal. Calc. for C<sub>52</sub>F<sub>10</sub>H<sub>62</sub>IrN<sub>6</sub>O<sub>8</sub>PSi<sub>2</sub>: C, 47.59; H, 4.76; N, 6.40. Best analyses found: C, 43.06; H, 4.89; N, 6.14 (fits well with **1**·2CH<sub>2</sub>Cl<sub>2</sub>). ESI (+): *m/z* 1223 [M]<sup>+</sup> (100%); 1195 [M-Et + H] (23%). IR (KBr, cm<sup>-1</sup>): ν(N-H) 3327 (vs); ν(C-H) 3270 (s), 3070 (s), 2959 (vs), 2930 (vs), 2875 (m); ν(C=O) 1670 (s); ν(C-H ring) 1604 (vs), 1558 (vs), 1479 (s), 1430 (s), 1405 (vs); ν(C-F) 1261 (s); ν(Si-O-C) 1163 (s), 1074 (vs); ν(P-F) 840 (vs). <sup>1</sup>H NMR (400 MHz, CDCl<sub>3</sub>, δ): 8.91 (s, 2H, H<sup>5'</sup><sub>bpy</sub>); 8.68 (s broad, NH); 8.34 (d, J<sub>H-H</sub> = 8.7 Hz, 2H, H<sup>2</sup><sub>dfppy</sub>); 8.05 (d, J<sub>H-H</sub> = 5.5 Hz, 2H, H<sup>2'</sup><sub>bpy</sub> or H<sup>3'</sup><sub>bpy</sub>); 7.97 (d, J<sub>H-H</sub> = 5.3 Hz, 2H, H<sup>2'</sup><sub>bpy</sub> or H<sup>3'</sup><sub>bpy</sub>); 7.83 (pst, J<sub>H-H</sub> = 6.6 Hz, 2H, H<sup>3</sup><sub>dfppy</sub>); 7.45 (d, J<sub>H-H</sub> = 5.5 Hz, 2H, H<sup>5</sup><sub>dfppy</sub>); 7.08 (pst, J<sub>H-H</sub> = 6.2 Hz, 2H, H<sup>4</sup><sub>dfppy</sub>); 6.60 (pst, <sup>3</sup>J<sub>F-H</sub> ≈ 10 Hz, 2H, H<sup>7</sup><sub>dfppy</sub>); 5.67 (dd, <sup>3</sup>J<sub>F-H</sub> ≈ 8 Hz, J<sub>H-H</sub> = 2 Hz, 2H, H<sup>9</sup><sub>dfppy</sub>); 3.82 (c, J<sub>H-H</sub> = 7.3 Hz, 12H, O-CH<sub>2</sub>CH<sub>3</sub>); 3.52 (m, 4H, CH<sub>2</sub>-CH<sub>2</sub>-CH<sub>2</sub>-Si); 1.81 (m, 4H, CH<sub>2</sub>CH<sub>2</sub>CH<sub>2</sub>-Si); 1.20 (t, J<sub>H-H</sub> = 7.0 Hz, 18H O-CH<sub>2</sub>CH<sub>3</sub>); 0.72 (m, 4H, CH<sub>2</sub>CH<sub>2</sub>CH<sub>2</sub>-Si). <sup>13</sup>C {<sup>1</sup>H} NMR (100.6 MHz, CDCl<sub>3</sub>, δ): 165.5 (s, C<sup>10</sup><sub>dfppy</sub>); 164.3 (s, C<sup>12</sup><sub>dfppy</sub>); 164.1 (d, J<sub>F-C</sub> = 230 Hz, C<sup>8</sup><sub>dfppy</sub>); 163.5 (s, CO); 161.5 (d, J<sub>F-C</sub> = 233 Hz, C<sup>6</sup><sub>dfppy</sub>); 155.8 (s, C<sup>4'</sup><sub>bpy</sub> or C<sup>6'</sup><sub>bpy</sub>); 150.8 (s, C<sup>2'</sup><sub>bpy</sub> or C<sup>3'</sup><sub>bpy</sub>); 148.6 (s, C<sup>5</sup><sub>dfppy</sub>); 146.5 (s, C<sup>4'</sup><sub>bpy</sub> or C<sup>6'</sup><sub>bpy</sub>); 139.6 (s, C<sup>3</sup><sub>dfppy</sub>); 128.1 (s, C<sup>2'</sup><sub>bpy</sub> or C<sup>3'</sup><sub>bpy</sub>); 127.5 (s broad, C<sup>11</sup><sub>dfppy</sub>); 124.0 (m, C<sup>2</sup><sub>dfppy</sub> or C<sup>4</sup><sub>dfppy</sub>); 122.6 (s, C<sup>5'</sup><sub>bpy</sub>); 114.2 (d, <sup>2</sup>J<sub>C-F</sub> ≈ 18 Hz, C<sup>9</sup><sub>dfppy</sub>); 99.9 (pst, J<sub>C-F</sub> ≈ 27 Hz, C<sup>7</sup><sub>dfppy</sub>); 58.6 (s, O-CH<sub>2</sub>CH<sub>3</sub>); 43.5 (s, CH<sub>2</sub>CH<sub>2</sub>CH<sub>2</sub>-Si); 22.8 (s, CH<sub>2</sub>CH<sub>2</sub>CH<sub>2</sub>-Si); 18.4 (s, O-CH<sub>2</sub>CH<sub>3</sub>); 7.9 (s, CH<sub>2</sub>CH<sub>2</sub>CH<sub>2</sub>-Si). <sup>19</sup>F {<sup>1</sup>H} NMR

(376.5 MHz, CDCl<sub>3</sub>,  $\delta$ ): -71.40 (d,  $J_{F-P} = 712$ ); -104.73 (d,  $J_{F-F} = 11.3$  Hz, 2F, F<sup>6</sup>); -107.91 (d,  $J_{F-F} = 11.2$  Hz, 2F, F<sup>8</sup>).

### Synthesis of *in-situ* mesoporous organometallo-silica nanoparticles (NP<sub>Me\_IS</sub>, NP<sub>OH\_IS</sub> and NP<sub>NH<sub>2</sub>\_IS</sub>)

The synthesis of the *in-situ* hybrid materials was carried out accomplishing the co-condensation of the silica precursor (TEOS) with the iridium complex **1**. In all the cases, the nominal metal concentration was 0.2 wt% (without considering the addition of DMDES or APTES), and the molar ratio of the synthesis gel was the following: 1.00 TEOS:  $6.6 \cdot 10^{-4}$  complex **1**: 0.060 CTAB: 0.026 TEA: 80.0 H<sub>2</sub>O (0.135 DMDES or 0.023 APTES, when appropriate).

**NP<sub>Me\_IS</sub>**. In a typical synthesis, 0.20 g (0.55 mmol) of CTAB (hexadecyltrimethylammonium bromide) was added to a mixture of 13.1 mL of distilled water and 31.4  $\mu$ L (0.24 mmol) of triethanolamine (TEA). The resulting suspension was heated up to 80°C for 1 hour. Simultaneously, a solution of complex **1** (7.9 mg,  $5.78 \cdot 10^{-3}$  mmol) in 3 mL of absolute ethanol and 1.90 g (9.12 mmol) of TEOS was stirred at room temperature. This last solution was added to that containing the surfactant at 80°C. After 10 minutes of reaction, 0.21 mL of diethoxydimethylsilane (DMDES, 1.22 mmol, capping agent) were added and the mixture was stirred until complete 2 hours of reaction. The mixture was cooled to room temperature and the particles were recovered by centrifugation (20 min at 20000 r.p.m.), and washed thoroughly with distilled water and ethanol. Finally, the surfactant was removed by ionic exchange with a saturated ammonium nitrate solution. **NP<sub>Me\_IS</sub>** was obtained as pale-yellow powder (0.36 g, 82%). IR (KBr, cm<sup>-1</sup>):  $\nu$ (O-H) 3475 (m broad), 1640 (w);  $\nu$ (C-H) 2968 (vw), 2928 (vw), 2852 (vw);  $\nu$ (ring) 1552 (vw), 1452 (vw), 1405 (vw);  $\nu$ (Si-CH<sub>3</sub>) 1267 (w), 850 (w);  $\nu$ (Si-O-Si) 1220, 1080 (s broad), 800 (w), 460 (m);  $\nu$ (Si-O) 950 (w).

**NP<sub>OH\_IS</sub>**. The synthesis was performed following the same procedure to that described for **NP<sub>Me\_IS</sub>**, but without the concurrence of the capping agent (DMDES). The particles were obtained as pale-yellow powder (0.39 g, 90%). IR (KBr, cm<sup>-1</sup>):  $\nu$ (O-H) 3475 (m broad), 1640 (w);  $\nu$ (C-H) 2927 (vw), 2854 (vw);  $\nu$ (Si-O-Si) 1220, 1080 (s broad), 800 (w), 460 (m);  $\nu$ (Si-O) 950 (w).

**NP<sub>NH<sub>2</sub>\_IS</sub>**. The same synthetic pathway to that described for **NP<sub>Me\_IS</sub>** was followed for the obtaining of these nanoparticles using, in this case, the capping agent (3-

aminopropyl)triethoxysilane (APTES, 48  $\mu\text{L}$ , 0.21 mmol). In this case, the resulting suspension obtained after the addition of the capping agent was reacted over 1 hour at 80°C. **NP<sub>NH<sub>2</sub></sub>\_IS** was obtained as pale-yellow powder (0.20 g, 36%). IR (KBr,  $\text{cm}^{-1}$ ):  $\nu(\text{O-H})$  3440 (m broad), 1640 (w);  $\nu(\text{N-H})$  3285 (m broad), 1390 (w);  $\nu(\text{C-H})$  2966 (vw), 2927 (vw), 2856 (vw);  $\nu(\text{ring})$  1536 (vw), 1475 (vw);  $\nu(\text{Si-O-Si})$  1220, 1080 (s broad), 800 (w), 460 (m);  $\nu(\text{Si-O})$  950 (w).

### ***Synthesis of mesoporous complex-free silica nanoparticles (NP<sub>OH</sub>, NP<sub>Me</sub> and NP<sub>NH<sub>2</sub></sub>)***

Complex-free mesoporous silica nanoparticles were prepared as white powder following the same procedure to that previously described for each *in-situ* materials, but without adding the metal complex (i–iv, Scheme S2).

**NP<sub>Me</sub>** (0.31 g, 68%). Molar ratio of the synthesis gel 1.00 TEOS: 0.060 CTAB: 0.026 TEA: 80.0 H<sub>2</sub>O: 0.135 DMDES. IR (KBr,  $\text{cm}^{-1}$ ):  $\nu(\text{O-H})$  3475 (m broad), 1640 (w);  $\nu(\text{Si-CH}_3)$  1267 (w), 850 (w);  $\nu(\text{Si-O-Si})$  1220, 1080 (s broad), 800 (w), 460 (m);  $\nu(\text{Si-O})$  950 (w).

**NP<sub>OH</sub>** (0.41 g, 76%). Molar ratio of the synthesis gel 1.00 TEOS: 0.060 CTAB: 0.026 TEA: 80.0 H<sub>2</sub>O. IR (KBr,  $\text{cm}^{-1}$ ):  $\nu(\text{O-H})$  3475 (m broad), 1640 (w);  $\nu(\text{Si-O-Si})$  1220, 1080 (s broad), 800 (w), 460 (m);  $\nu(\text{Si-O})$  950 (w).

**NP<sub>NH<sub>2</sub></sub>** (0.47 g, 81%). Molar ratio of the synthesis gel 1.00 TEOS: 0.060 CTAB: 0.026 TEA: 80.0 H<sub>2</sub>O: 0.023 APTES. IR (KBr,  $\text{cm}^{-1}$ ):  $\nu(\text{O-H})$  3440 (m broad), 1640 (w);  $\nu(\text{N-H})$  3285 (m broad), 1390 (w);  $\nu(\text{Si-O-Si})$  1220, 1080 (s broad), 800 (w), 460 (m);  $\nu(\text{Si-O})$  950 (w).

### ***Synthesis of grafted mesoporous organometallo-silica nanoparticles (NP<sub>Me</sub>\_G , NP<sub>OH</sub>\_G and NP<sub>NH<sub>2</sub></sub>\_G)***

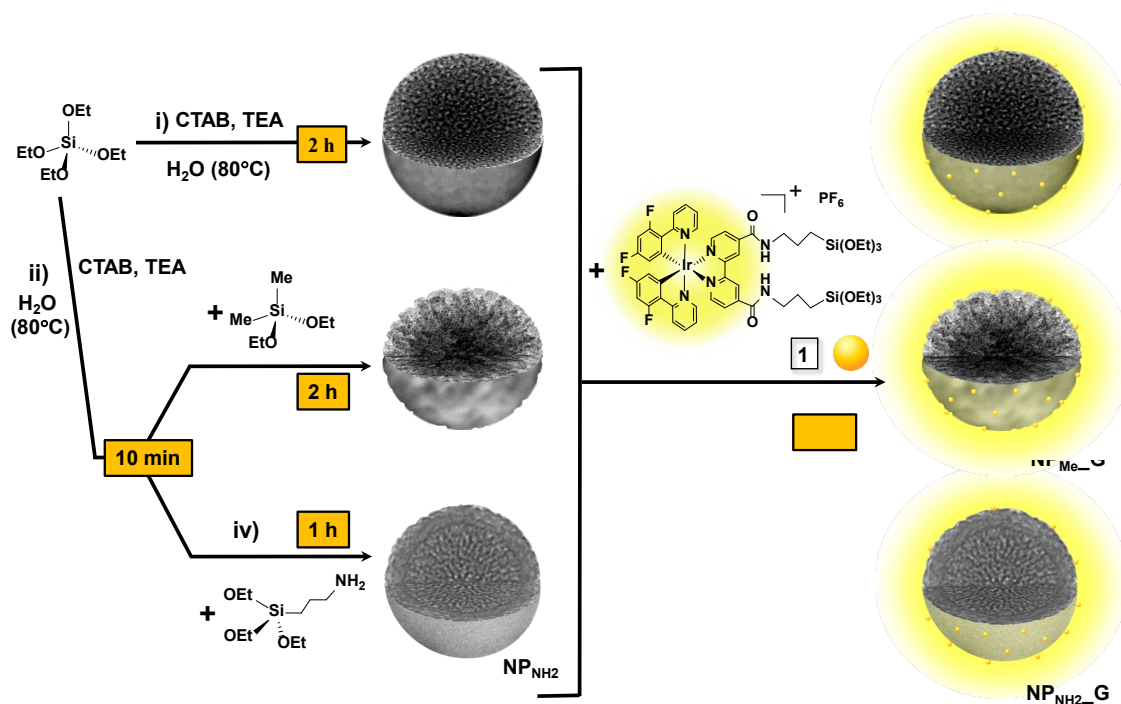
The synthesis of the grafted materials (v, Scheme S2) was carried out maintaining the same nominal molar ratio as in the hybrid *in-situ* silica nanoparticles. In a typical synthesis, 0.40 g (6.67 mmol) of the corresponding complex-free silica nanoparticles (**NP<sub>OH</sub>**, **NP<sub>Me</sub>** or **NP<sub>NH<sub>2</sub></sub>**) were suspended in 30 mL of ethanol. A solution of 5.8 mg (4.2 mmol) of complex **1** in 3 mL of ethanol was added dropwise and the mixture was stirred during 3 hours until a homogeneous distribution was provided. Subsequently, 1 mL of an aqueous solution 0.05M of NaF was added, and the resulting mixture was kept under

magnetic stirring for 24 hours at room temperature. The yellow solids obtained were centrifuged and washed thoroughly with ethanol.

**NP<sub>Me</sub>\_G** (0.31 g, 77%). IR (KBr, cm<sup>-1</sup>): ν(O-H) 3450 (m broad), 1640 (w); ν(C-H) 2969 (vw), 2029 (vw), 2854 (vw); ν(ring) 1554 (vw), 1454 (vw), 1406 (vw); ν(Si-CH<sub>3</sub>) 1264 (w), 845 (w); ν(Si-O-Si) 1220 (m), 1090 (vs broad), 800 (w), 460 (m); ν(Si-O) 950 (w).

**NP<sub>OH</sub>\_G** (0.36 g, 87%). IR (KBr, cm<sup>-1</sup>): ν(O-H) 3450 (m broad), 1640 (w); ν(C-H) 2929 (vw), 2858 (vw); ν(ring) 1554 (vw), 1479 (vw); ν(Si-O-Si) 1220, 1090 (s broad), 800 (w), 460 (m); ν(Si-O) 950 (m).

**NP<sub>NH<sub>2</sub></sub>\_G** (0.34g, 85%). IR (KBr, cm<sup>-1</sup>): ν(O-H) 3430 (m broad), 1640 (w); ν(N-H) 3280 (m broad), 1390 (w); ν(C-H) 2962 (vw), 2025 (vw), 2854 (vw); ν(ring) 1533 (vw), 1467 (vw); ν(Si-O-Si) 1220, 1080 (vs broad), 800 (w), 460 (m); ν(Si-O) 950 (w).



**Scheme S2.** Schematic representation of the synthesis of the control mesoporous silica nanoparticles (NP<sub>OH</sub>, NP<sub>Me</sub>, and NP<sub>NH<sub>2</sub></sub>) and the grafted mesoporous organometallo-silica nanoparticles (NP<sub>OH</sub>\_G, NP<sub>Me</sub>\_G and NP<sub>NH<sub>2</sub></sub>\_G).

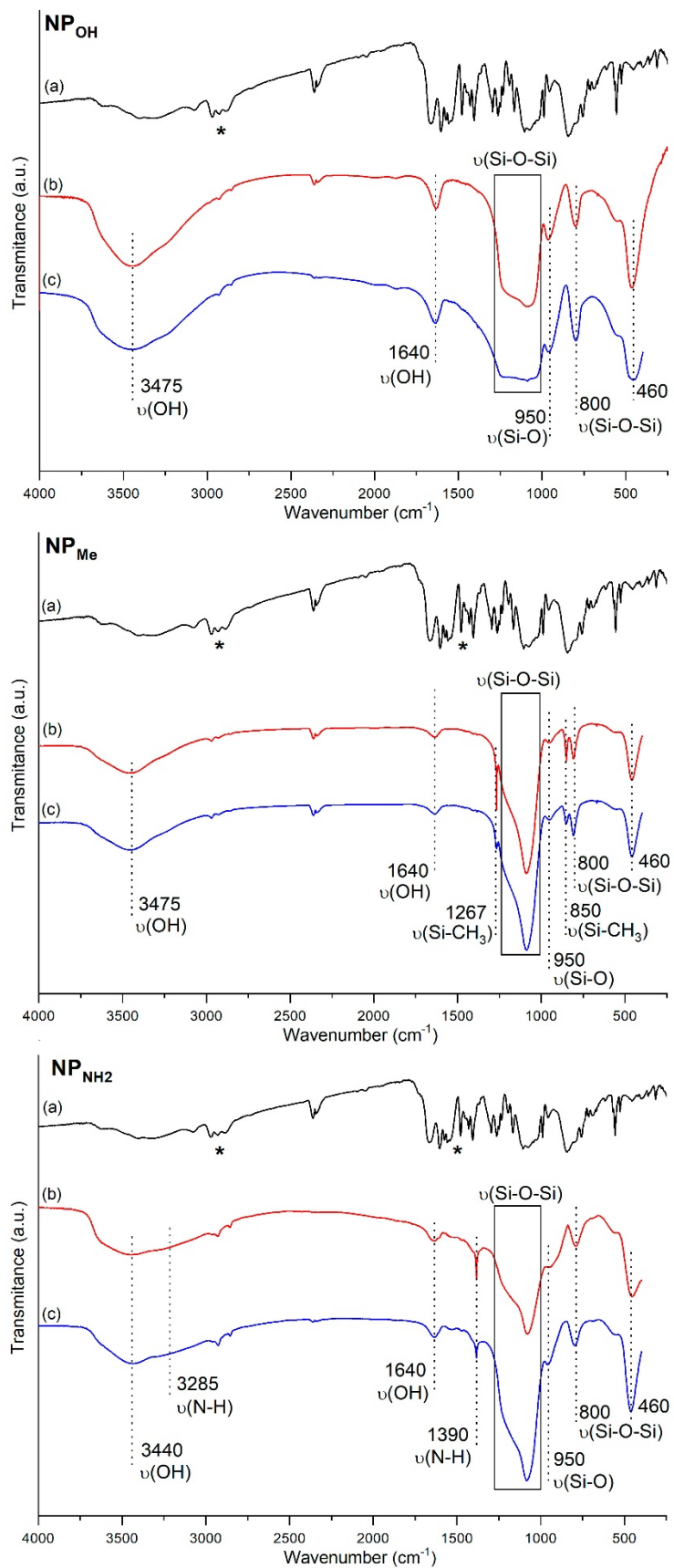


**Figure S1.** FTIR spectra of the *in situ* (IS, b) and the *grafted* (G, c) silica NPs in comparison with the spectra of the pure complex **1** (a). (\*) Characteristic absorption of the complex observed in the hybrid materials.

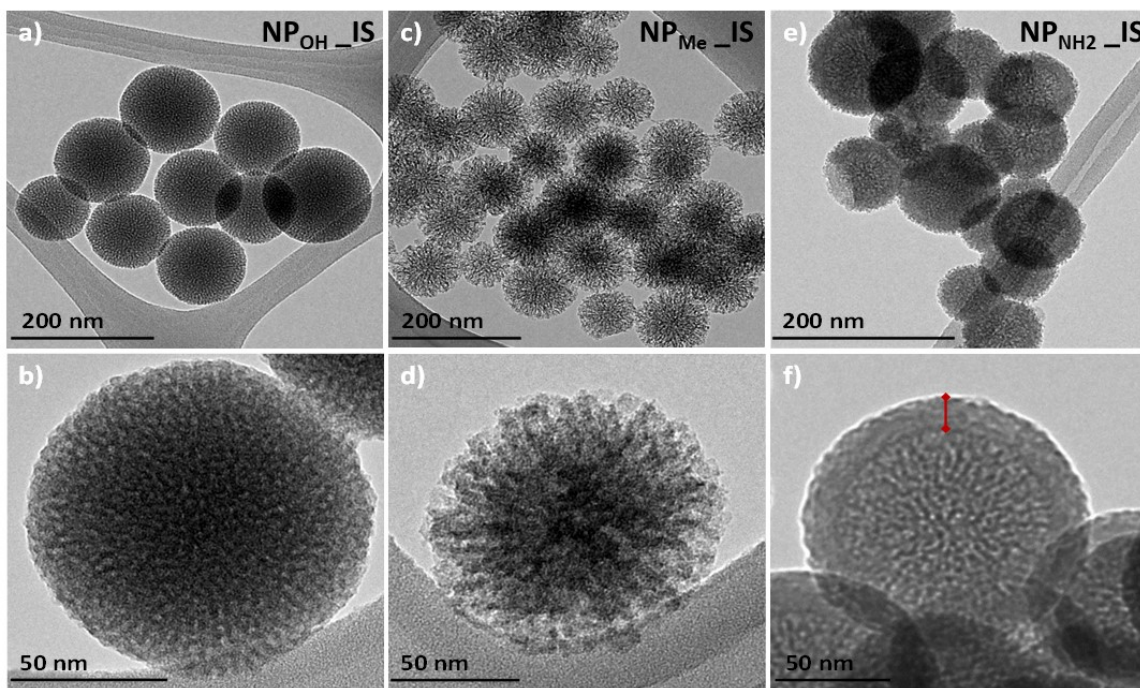


**Figure S2.** Representative TEM images of the hybrid *in-situ* NPs at two different magnification: (a,b)  $\text{NP}_{\text{OH\_IS}}$ , (c,d)  $\text{NP}_{\text{Me\_IS}}$ , (e,f)  $\text{NP}_{\text{NH}_2\_IS}$ .  $\text{NP}_{\text{NH}_2\_IS}$  show a disorderer corona shell of *ca.* 16 nm thick (double arrowhead line in f).

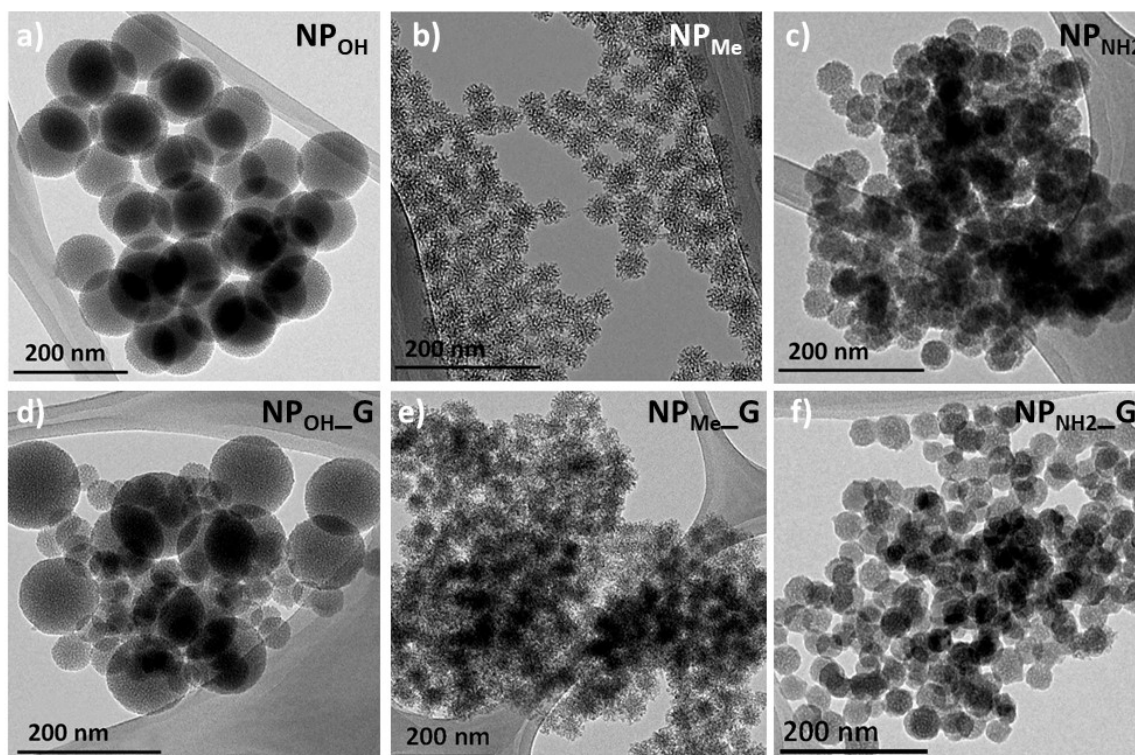


**Figure S3.** Representative TEM images of the control NPs (upper part): (a)  $\text{NP}_{\text{OH}}$ , (b)  $\text{NP}_{\text{Me}}$ , (c)  $\text{NP}_{\text{NH}_2}$ ; and the grafted NPs (bottom): (d)  $\text{NP}_{\text{OH\_G}}$ , (e)  $\text{NP}_{\text{Me\_G}}$ , (f)  $\text{NP}_{\text{NH}_2\_G}$ .

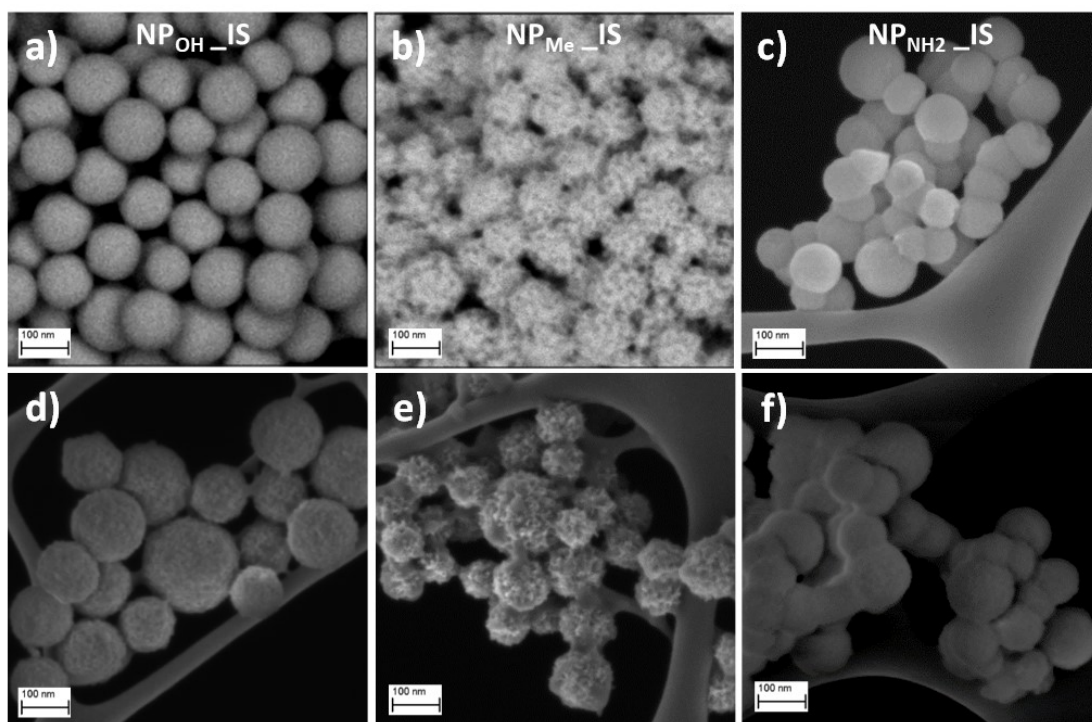


**Figure S4.** Representative FESEM images of the of freshly prepared hybrid *in-situ* NPs: (a)  $\text{NP}_{\text{OH\_IS}}$ , (b)  $\text{NP}_{\text{Me\_IS}}$ , (c)  $\text{NP}_{\text{NH}_2\_IS}$  (upper part), and after six months suspended in complete RPMI cell culture medium: (d)  $\text{NP}_{\text{OH\_IS}}$ , (e)  $\text{NP}_{\text{Me\_IS}}$ , (f)  $\text{NP}_{\text{NH}_2\_IS}$  (bottom).

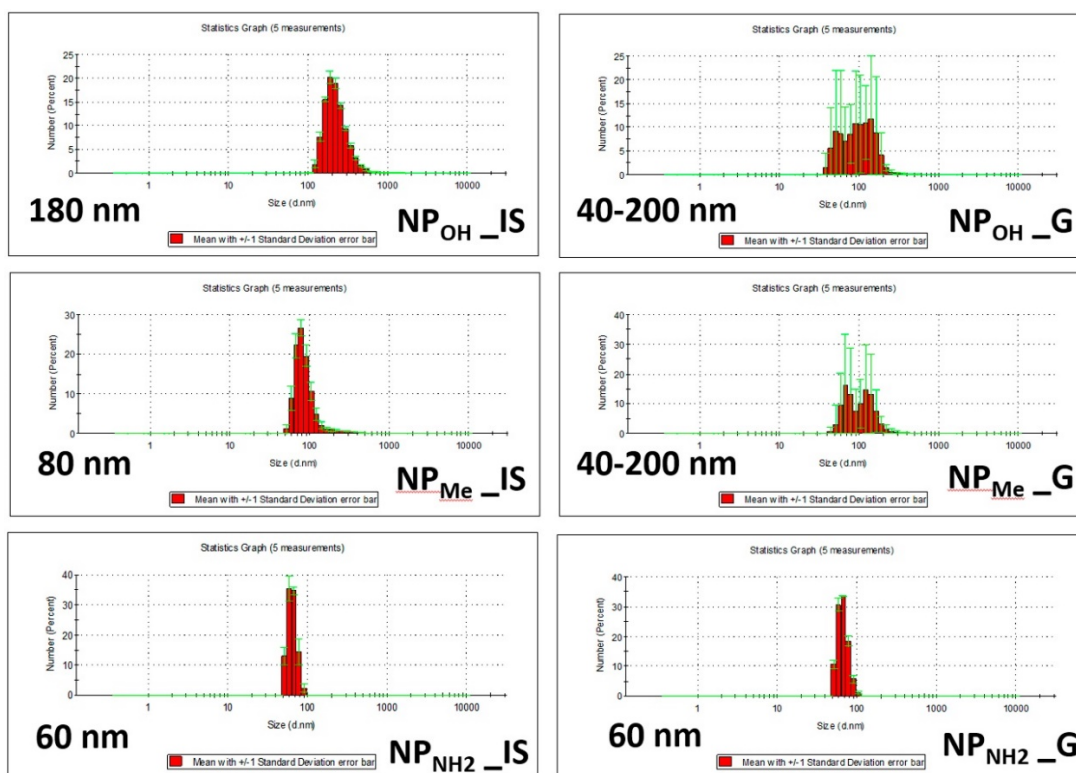


**Figure S5.** DLS size distribution of all the hybrid organometallo-silica NPs including the *in-situ* (IS, left) and **grafted** (G, right) materials.

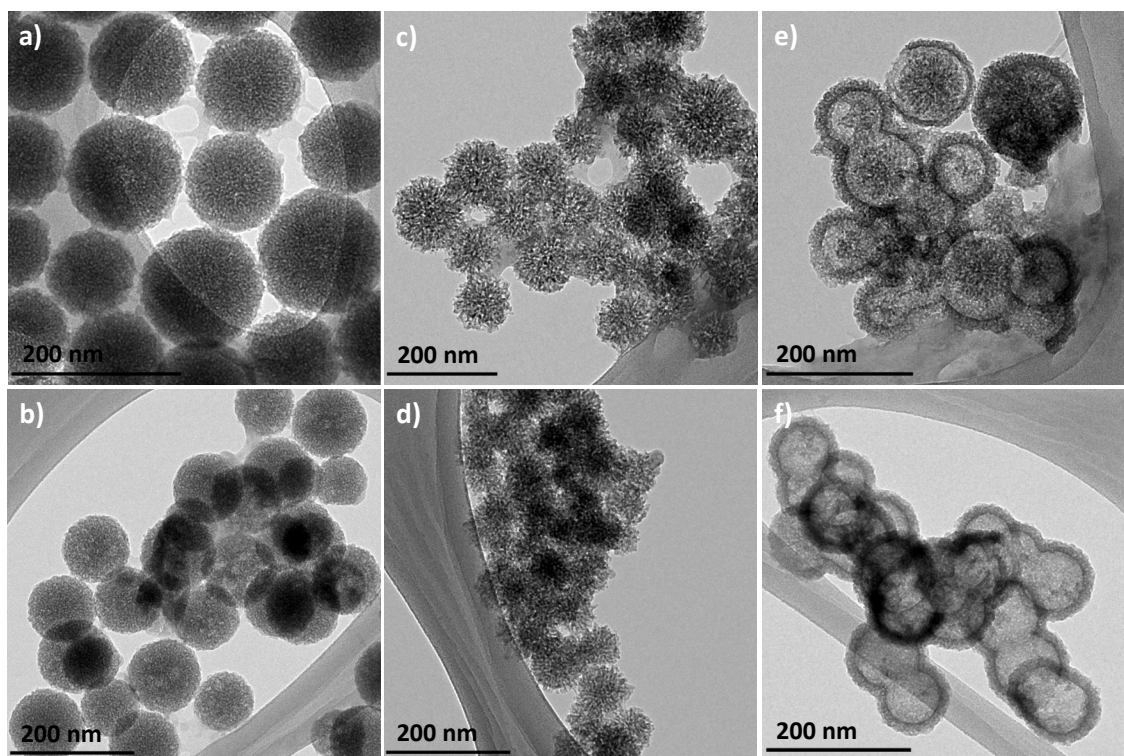


**Figure S6.** Representative TEM images of the hybrid NPs after six months suspended in a complete physiologic medium. *in-situ* (upper part): (a)  $\text{NP}_{\text{OH\_IS}}$ , (c)  $\text{NP}_{\text{Me\_IS}}$ , (e)  $\text{NP}_{\text{NH}_2\_IS}$ ; and grafted (bottom): (b)  $\text{NP}_{\text{OH\_G}}$ , (d)  $\text{NP}_{\text{Me\_G}}$ , (f)  $\text{NP}_{\text{NH}_2\_G}$ .

**Photophysical Properties of complex 1 and nanoparticles.**

**Table S1.** Absorption data for complex 1 (solution  $5 \times 10^{-5}$  M) and the organometallo-silica NPs.

Sample	$\lambda_{\text{abs}}/\text{nm}$ ( $\epsilon \times 10^{-3}/\text{M}^{-1} \text{cm}^{-1}$ )
	285, 312, 380, 420, 445, 476 <i>Solid</i>
$[\text{Ir}(\text{dfppy})_2(\text{dasipy})]\text{PF}_6$ (1)	260 (54.0), 274 <sub>sh</sub> (47.9), 305 (31.6), 360 (8.8), 417 (1.1), 445 (0.8), 470 (0.4) <i>THF</i>
$\text{NP}_{\text{OH\_IS}}$	265, 284, 310, 350, 420, 445 <i>Solid</i>
$\text{NP}_{\text{OH\_G}}$	270, 288, 307, 350, 422, 447, 476 <i>Solid</i>
$\text{NP}_{\text{Me\_IS}}$	305, 350, 418, 445 <i>Solid</i>
$\text{NP}_{\text{Me\_G}}$	266, 290, 305, 348, 419, 448 <i>Solid</i>
$\text{NP}_{\text{NH}_2\_IS}$	215, 270, 308, 357, 418, 450 <i>Solid</i>
$\text{NP}_{\text{NH}_2\_G}$	215, 267, 290, 307, 351, 419, 448 <i>Solid</i>

**Table S2.** Photophysical data for complex **1** (solutions  $5 \times 10^{-4}$  M) and the organometallosilica NPs (aqueous suspension  $5 \times 10^{-4}$  M). Radiative ( $K_r$ ) and non-radiative ( $K_{nr}$ ) constants calculated at room temperature.

Sample	Medium (T/K)	$\lambda_{em}/\text{nm}$ ( $\lambda_{exc}/\text{nm}$ ) <sup>a)</sup>	$\Delta E(T_1-S_0)$ (nm) <sup>b)</sup>	$\tau/\mu\text{s}$ <sup>c)</sup>	$\phi/\%$	$K_r$	$K_{nr}$
<b>1</b>	Solid (298)	560		0.35	29.4 <sup>d)</sup>	$8.4 \cdot 10^5$	$2.0 \cdot 10^6$
	Solid (77)	550 <sub>max</sub> , 580		11.8			
	THF (298)	550	575	0.71	55.8 <sup>d)</sup>	$7.9 \cdot 10^5$	$6.2 \cdot 10^5$
	THF (77)	510		8.10			
	MeOH (298)	585	587	0.40	66.4 <sup>d)</sup>	$1.7 \cdot 10^6$	$8.0 \cdot 10^5$
	MeOH (77)	530		7.60			
<b>NP<sub>OH</sub>_IS</b>	Solid <sup>e)</sup>	552		0.69	41.2 <sup>f)</sup>	$6.0 \cdot 10^5$	$8.5 \cdot 10^5$
	Suspension <sup>e)</sup>	550			25.8 <sup>f)</sup>		
<b>NP<sub>Me</sub>_IS</b>	Solid <sup>e)</sup>	550		0.72	50.1 <sup>f)</sup>	$7.0 \cdot 10^5$	$6.9 \cdot 10^5$
	Suspension <sup>e)</sup>	550			39.6 <sup>f)</sup>		
<b>NP<sub>NH2</sub>_IS</b>	Solid <sup>e)</sup>	558		0.80	52.0 <sup>d)</sup>	$6.5 \cdot 10^5$	$6.0 \cdot 10^5$
	Suspension <sup>e)</sup>	553			27.5 <sup>f)</sup>		
<b>NP<sub>OH</sub>_G</b>	Solid <sup>e)</sup>	550		0.52	28.4 <sup>d)</sup>	$5.5 \cdot 10^5$	$1.46 \cdot 10^6$
	Suspension <sup>e)</sup>	570			18.5 <sup>f)</sup>		
<b>NP<sub>Me</sub>_G</b>	Solid <sup>e)</sup>	545		0.56	39.2 <sup>d)</sup>	$7.0 \cdot 10^5$	$1.1 \cdot 10^6$
	Suspension <sup>e)</sup>	570			26.1 <sup>f)</sup>		
<b>NP<sub>NH2</sub>_G</b>	Solid <sup>e)</sup>	545		0.64	41.4 <sup>d)</sup>	$6.5 \cdot 10^5$	$9.1 \cdot 10^5$
	Suspension <sup>e)</sup>	565			17.3 <sup>f)</sup>		

a) Data measured with  $\lambda_{exc}$  at 365 nm. Similar emission spectra obtained by excitation in the range 365 – 480 nm. b) Calculated emissions considering the corresponding solvents. c) Emissions lifetimes calculated as average of a bi-exponential decay. Low temperature measurements calculated as mono-exponential decay. d)  $\lambda_{exc}$  at 440 nm. e) Data measured at 298 K. f)  $\lambda_{exc}$  at 365 nm.

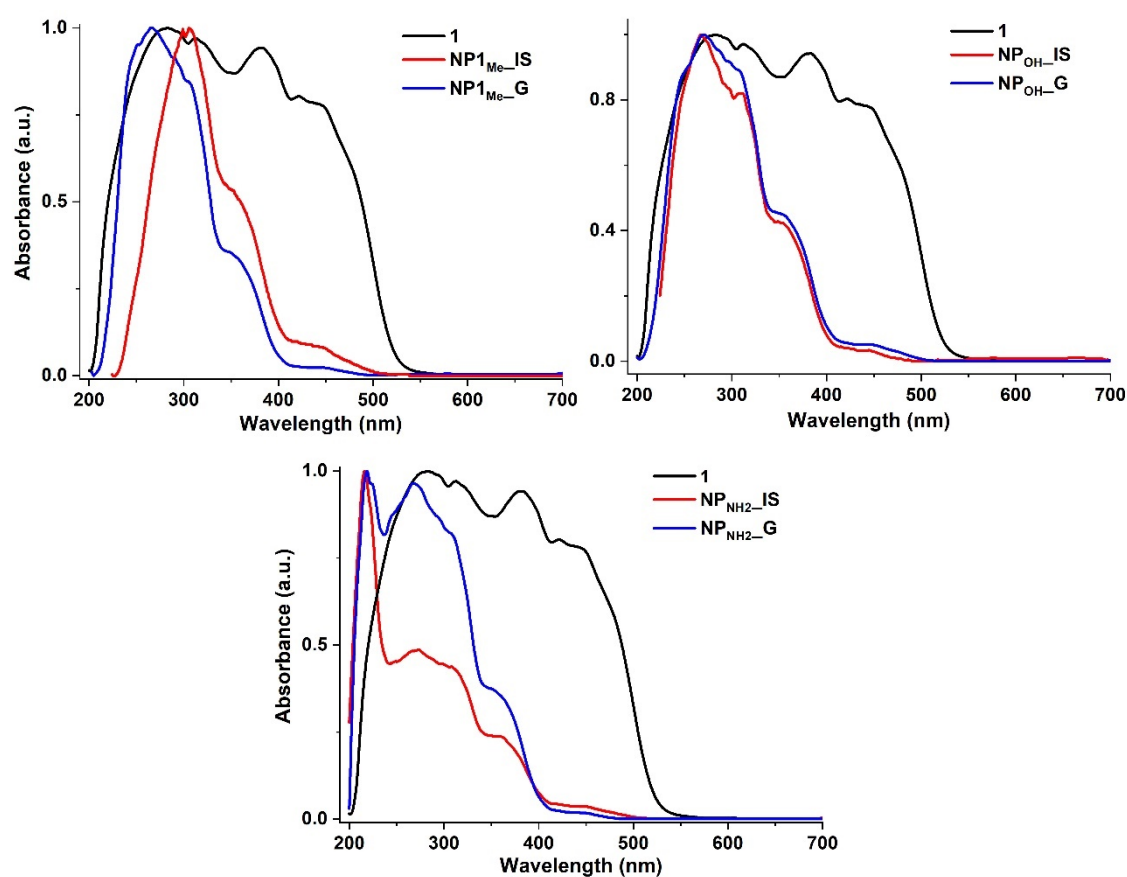


**Fig. S7.** Solid state DRUV spectrum of complex **1** compared with those of the organometallo-silica NPs ( $\text{NP}_{\text{Me\_IS,G}}$ ;  $\text{NP}_{\text{OH\_IS,G}}$ ;  $\text{NP}_{\text{NH}_2\_IS,G}$ ).

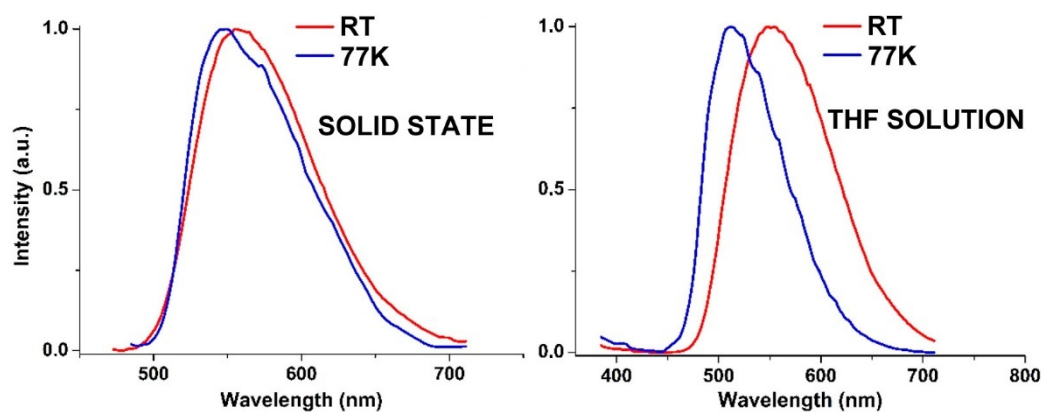


**Fig. S8.** Emission spectra ( $\lambda_{\text{exc}}$  365 nm) of complex **1** in solid state (left) and in THF solution (right,  $5 \times 10^{-4}$  M), at room temperature and at 77K.

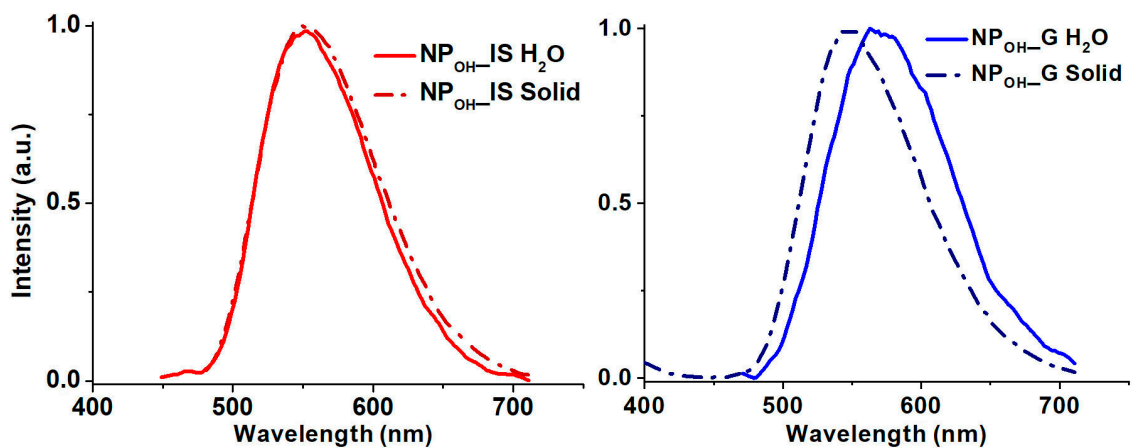


**Fig. S9.** Emission spectra at room temperature of  $\text{NP}_{\text{OH\_IS}}$  (left, in red) and  $\text{NP}_{\text{OH\_G}}$  (right, in blue) in solid state (dotted line) and in water suspension (solid line).

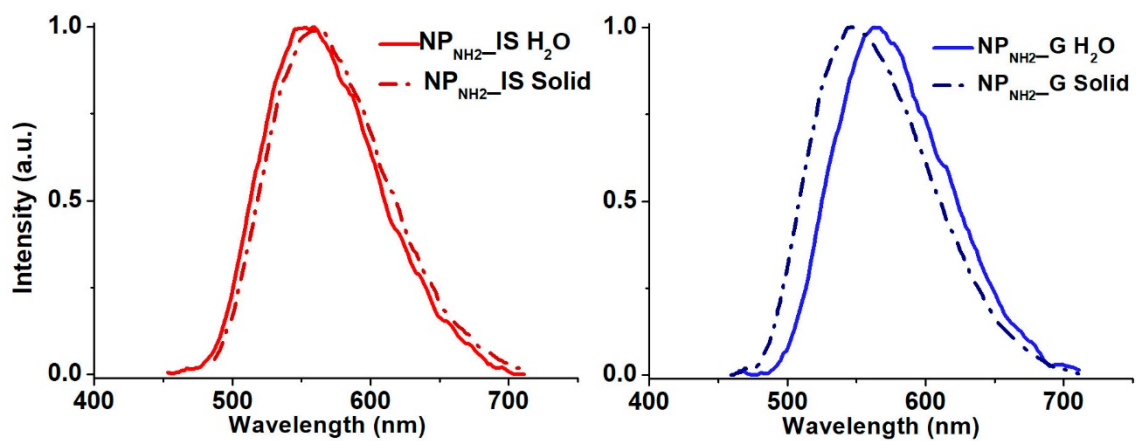


**Fig. S10.** Emission spectra at room temperature of  $\text{NP}_{\text{NH}_2\_IS}$  (left, in red) and  $\text{NP}_{\text{NH}_2\_G}$  (right, in blue) in solid state (dotted line) and in water suspension (solid line).

### Theoretical calculations

Calculations for complex **1** (THF solution) were carried out with the Gaussian 09 package,<sup>4</sup> using Becke's three-parameter functional combined with Lee-Yang-Parr's correlation functional (B3LYP) in the singlet state ( $S_0$ ), and the unrestricted U-B3LYP in the triplet state ( $T_1$ ).<sup>5</sup> According to previous theoretical calculations for iridium complexes, the optimized ground state geometry were calculated at the B3LYP/LANL2DZ (Ir)/6-31G(d,p) (ligands' atoms) level. The  $S_0$  geometry was found to be a true minimum as no negative frequencies in the vibrational frequency study of the final geometry were found. DFT and TD-DFT calculations were carried out using the polarized continuum model approach<sup>6</sup> implemented in the Gaussian 09 software. The MO diagrams and the orbital contributions were generated with Gaussian 09 software and Gauss-Sum<sup>7</sup> program, respectively. The emission energy was calculated as the difference of the optimized  $T_1$  geometry for both states (adiabatic electronic transition).

**Table S3.** DFT optimized geometries for ground state and triplet state of complex **1**.

	<b>1</b>	
	<b>S<sub>0</sub></b>	<b>T<sub>1</sub></b>
Ir(1)-N(1)	2.081	2.080
Ir(1)-N(1')	2.082	2.080
Ir(1)-C(10)	2.021	2.000
Ir(1)-C(10')	2.022	1.999
Ir(1)-N(a)	2.204	2.191
Ir(1)-N(a')	2.202	2.182
N(1)-Ir(1)-N(1')	173.60	176.20
N(1)-Ir(1)-C(10)	80.09	80.96
N(1')-Ir(1)-C(10')	80.06	80.90
N(1)-Ir(1)-C(10')	95.37	96.53
N(1')-Ir(1)-C(10)	95.30	96.46
N(a)-Ir(1)- N(a')	75.02	75.39
N(a)-Ir(1)-N(1)	88.15	86.93
N(a)-Ir(1)-C(10)	98.00	94.38
N(a)-Ir(1)-N(1')	96.93	96.07
N(a)-Ir(1)-C(10')	172.39	170.10
N(a')-Ir(1)-N(1)	97.27	95.49
N(a')-Ir(1)-C(10)	172.68	169.39
N(a')-Ir(1)-N(1')	87.85	87.55
N(a')-Ir(1)-C(10')	97.80	95.01

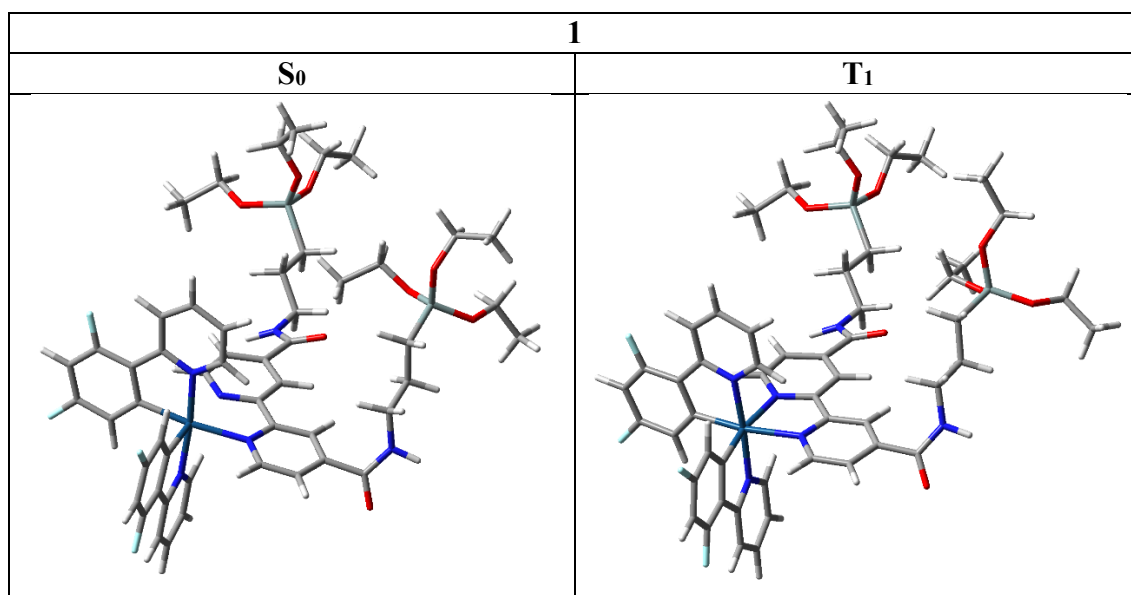
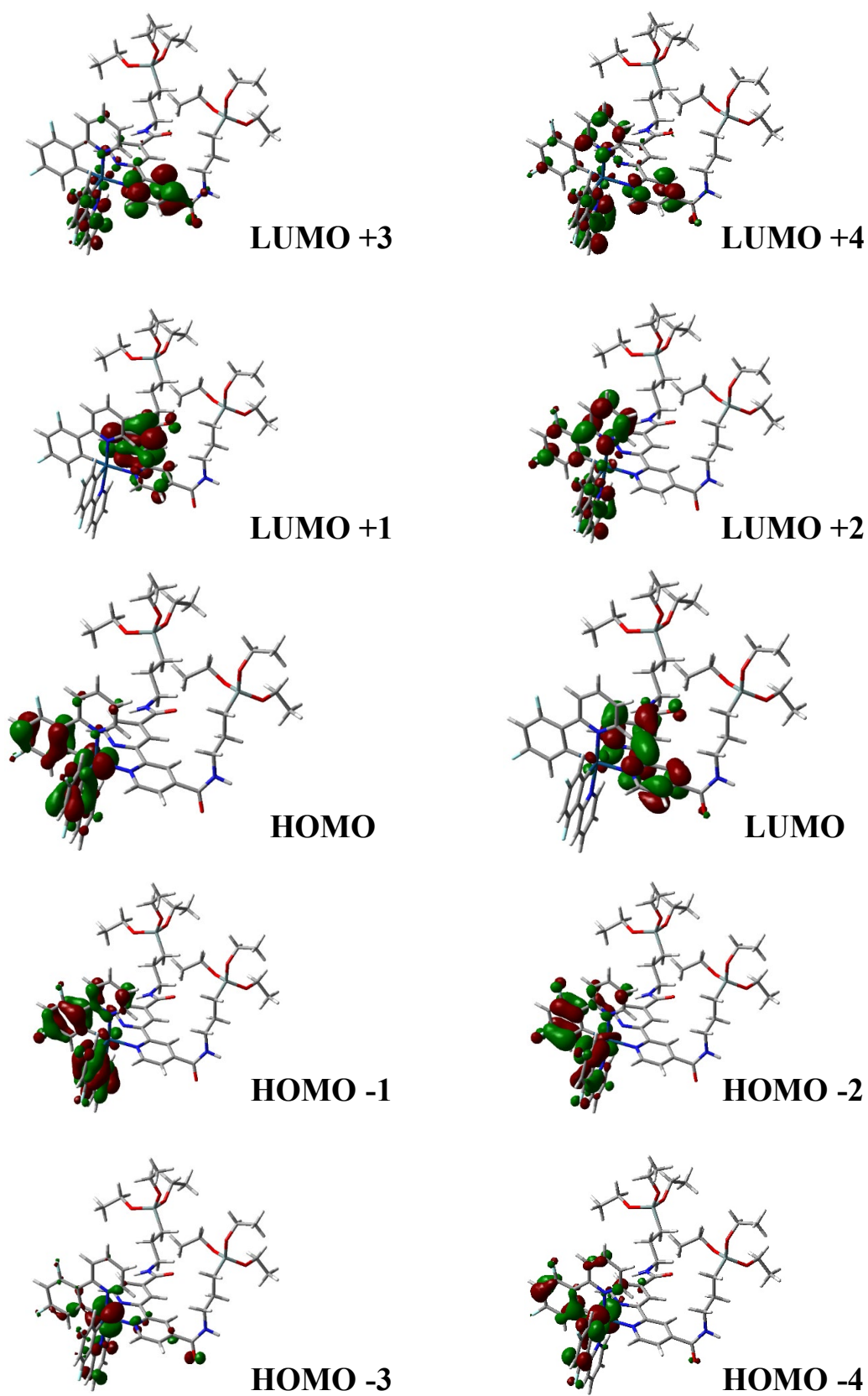


Fig. S11. Optimized structures of S<sub>0</sub> and T<sub>1</sub> states of **1**.

Table S4. Composition (%) of Frontier MOs in the ground state for complex **1** in THF.

	1				
	eV	dfppy (1)	dfppy (2)	dasipy	Ir
LUMO+5	-1.47	25	68	5	2
LUMO+4	-2.04	41	26	31	2
LUMO+3	-2.09	26	6	65	3
LUMO+2	-2.14	29	64	3	4
LUMO+1	-2.27	1	2	96	1
LUMO	-3.09	0	0	96	3
HOMO	-6.24	32	30	2	36
HOMO-1	-6.68	52	41	1	6
HOMO-2	-6.79	39	49	1	11
HOMO-3	-7.06	17	11	10	61
HOMO-4	-7.09	24	28	8	41
HOMO-5	-7.17	32	37	7	25



**Figure S12.** Selected frontier Molecular Orbitals for complex 1.

**Table S5.** Selected vertical excitation energies singlets ( $S_0$ ) and first triplets computed by TDDFT/SCRF (THF) with the orbitals involved for complex **1**.

State	$\lambda_{ex}(nm)$	f	Major transition (% Contribution)	Main Character
T <sub>1</sub>	505.70	---	HOMO→LUMO (97%)	ML'CT/LL'CT
T <sub>2</sub>	432.66	---	H-3→LUMO (43%), H-2→LUMO (11%)	ML'CT/LL'CT
T <sub>3</sub>	428.80	---	H-2→L+2 (11%), H-1→L+4 (15%), HOMO→L+2 (47%)	LL'CT/ML'CT/IL
T <sub>5</sub>	421.86	---	H-5→LUMO (14%), H-4→LUMO (22%), H-1→LUMO (42%)	LL'CT/ML'CT
S <sub>1</sub>	499.49	0.0005	HOMO→LUMO (99%)	ML'CT/LL'CT
S <sub>2</sub>	404.92	0.0213	H-1→LUMO (95%)	LL'CT
S <sub>3</sub>	400.57	0.0031	H-3→LUMO (31%), H-2→LUMO (62%)	ML'CT/LL'CT
S <sub>6</sub>	369.41	0.0824	H-4→LUMO (58%), HOMO→L+1 (22%)	ML'CT/LL'CT
S <sub>7</sub>	366.83	0.0301	H-4→LUMO (11%), HOMO→L+1 (70%)	ML'CT/LL'CT
S <sub>19</sub>	307.81	0.0770	H-2→L+2 (16%), H-1→L+3 (43%), H-1→L+4 (18%)	LL'CT/IL/ML'CT
S <sub>38</sub>	280.83	0.2825	H-5→L+2 (15%), H-4→L+4 (19%), H-1→L+2 (11%)	IL/MLCT
S <sub>52</sub>	262.23	0.1920	H-2→L+5 (37%), HOMO→L+8 (28%)	IL
S <sub>57</sub>	255.38	0.2356	H-1→L+6 (10%), HOMO→L+6 (13%), HOMO→L+8 (20%)	IL/MLCT

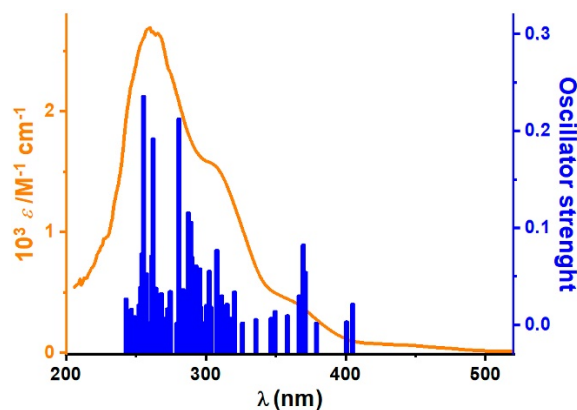
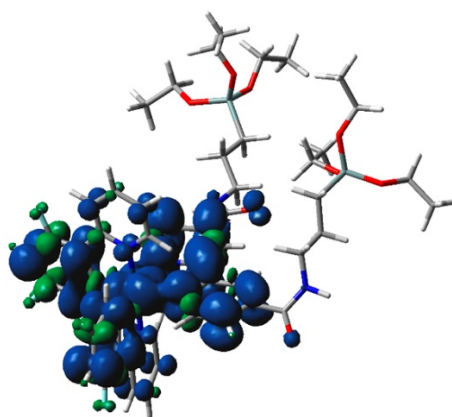


**Figure S13.** Calculated stick absorption spectra of complexes **1** in THF compared with the experimental one.



*Spin density on Ir: 0.5039*

**Figure S14.** Spin-density distributions calculated for the emitting excited state ( $T_1$ ) of complex **1**.

## **Biological Procedures**

### ***Cell lines and culture conditions***

A549 (adenocarcinomic alveolar basal epithelial cells) and HeLa (epitheloid cervix carcinoma cells) human cell lines were cultured following the American Type Culture Collection ([www.atcc.org](http://www.atcc.org)) recommendations and standard methods, as previously described.<sup>8</sup> Cells were maintained in RPMI 1640 medium supplemented with 10% fetal bovine serum (FBS), penicillin (100 U/mL) and streptomycin (100 µg/mL), kept under a humidified atmosphere of 95% air/5% CO<sub>2</sub> at 37°C, and sub-cultured before they get confluent using a 0.25% trypsin-EDTA solution.

### ***Localization in cells by fluorescence microscopy***

*In-vivo* cytolocalization of NP<sub>Me</sub>\_IS and NP<sub>OH</sub>\_IS nanoparticles in A549 and HeLa cells was performed as previously reported.<sup>9</sup> In brief, cells were cultured over one cm diameter poly- L-lysine-coated (Sigma-Aldrich) coverslips into a 24-well plate in 0.5 mL of supplemented culture medium per well for 48 h. Then, 0.5 mL of medium containing each nanoparticle at 50 µg/mL was added and cells were incubated o/n at 37°C. Following, 3.2 µM of Hoechst 33258 (Sigma-Aldrich) was added to the medium for 1 h at 37°C. Medium was removed and cells were washed twice with phosphate buffer saline (PBS, pH 7.2). As a control to discard emission bleeding between light channels, the incubation of cells was also performed separately with Hoechst alone. Coverslips were removed from plates and mounted on glass slides before being immediately examined under a fluorescence microscope (Leica DM600B). The microscope was equipped with a Nomarski differential interference contrast for transmitted light, and with an incident light fluorescence illuminator accommodating three filter cubes (N2.1:  $\lambda_{ex}$  filter BP 515-560, dichromatic mirror 580, suppression filter  $\lambda_{em}$  LP 590, green; Y5:  $\lambda_{ex}$  filter BP 620/60, dichromatic mirror 660, suppression filter  $\lambda_{em}$  BP 700/75, red; and A4:  $\lambda_{ex}$  filter BP 360/40, dichromatic mirror 400, suppression filter  $\lambda_{em}$  BP 470/40, blue) (Leica), suitable for imaging switching between Nomarski DIC transmitted light, and green, red and blue fluorescent light channels. Images of the living cells were documented using a 40x objective (Leica PLAN APO), a B&W digital camera (Hamamatsu ORCA R2, mod. C10600) and additional 2.5x digital zoom with the help of Micro-Manager Open Source Microscopy Software and Fiji/ImageJ free software.<sup>10</sup>

### ***Cellular uptake and cytolocalization: cell treatment, immunocytochemistry and confocal microscopy***

A549 and HeLa cells were cultured over one cm diameter poly-L-lysine-coated (Sigma-Aldrich) coverslips into a 24-well plate in 0.5 mL of supplemented culture medium per well for 48 h. Then, 0.5 mL of medium containing each *in-situ* or grafted silica nanoparticle at 75-100  $\mu\text{g}/\text{mL}$  were added and cells incubated 24 h at 37 °C. Following, cells were washed twice with phosphate buffer saline (PBS, pH 7.2) and fixed in 4% paraformaldehyde in PBS for 15 minutes. For immunocytochemical fluorescent staining, cells were permeabilized with 0.5% IGEPAL (Sigma- Aldrich) and 100 mM glycine in PBS (pH 7.4), washed with PBS, blocked with 5% FBS in PBS, and exposed to a mouse monoclonal anti- $\beta$ -tubulin primary antibody (clone TUB 2.1; Sigma- Aldrich) (1:1000 dilution in blocking solution) overnight at 4°C to specifically label microtubules. The following day, after three washes in 0.02% Tween-20 (Sigma-Aldrich) in PBS, Cy3 goat S9 antimouse IgGs (Jackson Immuno Research) (1:400 dilution in blocking solution), which bind anti-tubulin IgGs, were added to the cells for 2 h. Finally, after three PBS washes, coverslips were placed on glass slides using ProLong Gold Antifade Reagent (Molecular Probes) containing 4',6-diamidino-2-phenylindole (DAPI) (Molecular Probes) as a nuclear counterstain. Slides were examined under a confocal microscope (TCS SP5, Leica Microsystems, Mannheim; Germany) and documented using a 63x oil immersion objective and additional 4x digital zoom with help of LAS AF Lite microscopy software (Leica Microsystems). Images were projected into a single layer and the resulting two-dimensional data set was merged using the Fiji/ImageJ Open Source image processing software package.<sup>8c</sup>

### ***Cytotoxicity assay.***

The MTS (3-(4,5-dimethylthiazol-2-yl)-5-(3-carboxymethoxyphenyl)-2-(4-sulfophenyl)-2H-tetrazolium) hydrolysis method (MTS-based CellTiter® 96. AQueous Assay; Promega Corp., Madison, WI) was used to determine the cell viability as an indicator of A549 and HeLa cells sensitivity to the organometallo-silica nanoparticles as previously reported for other compounds.<sup>8, 11</sup> Briefly, 50  $\mu\text{L}$  of exponentially growing cells were seeded at a density of  $1.5 \times 10^3$  cells per well, in a 96-well flat-bottomed microplate in growing media, with reduced concentrations of FBS (5%) in case of A549. 24 h later they were incubated for 72 h with the nanoparticles. *In-situ* (NP<sub>Me</sub>\_IS, NP<sub>OH</sub>\_IS

and NP<sub>NH<sub>2</sub></sub>\_IS) and grafted (NP<sub>Me</sub>\_G, NP<sub>OH</sub>\_G and NP<sub>NH<sub>2</sub></sub>\_G) silica nanoparticles in stock solutions were resuspended in water (1.5-3.5 mg/mL) and dissolved in test medium as nine 1:1.5 serial dilutions for both cell lines. 50 µL of each dilution or medium alone was added to growing cells in the 96-well plate designed as previously recommended.<sup>12</sup> Final concentrations in sextuplicates ranged from 200 to 9.75 µg/mL for both cell lines, except NP<sub>OH</sub>\_G for A549 cells and NP<sub>NH<sub>2</sub></sub>\_G for HeLa cells that was from 500 to 9.75 µg/mL. After 72 h at 37 °C, 20 µl of MTS was added and plates were incubated for 1 h at 37 °C. Finally, the optical density was measured at 490 nm using a 96-well multiscanner autoreader (POLARstar Omega, BMG Labtech; Germany). Each experiment was repeated three times. The IC<sub>50</sub> (nanoparticles concentration that produced 50% inhibition of cell proliferation) was calculated by plotting percentage of growing inhibition versus log of the nanoparticles concentration using the GraphPad Prism 6 (La Jolla, CA) software.

In order to test if cytotoxicity could be affected by nanoparticle storage and instability, the nine 1:1.5 serial dilutions of NP<sub>Me</sub>\_G, NP<sub>OH</sub>\_G, NP<sub>NH<sub>2</sub></sub>\_G and NP<sub>NH<sub>2</sub></sub>\_IS used for HeLa cells were stored in complete cell culture medium for 6 months at 4°C. After this time, 50 µL of each dilution or medium alone was added to growing HeLa cells in the 96-well plate and the MTS assay performed as described above.

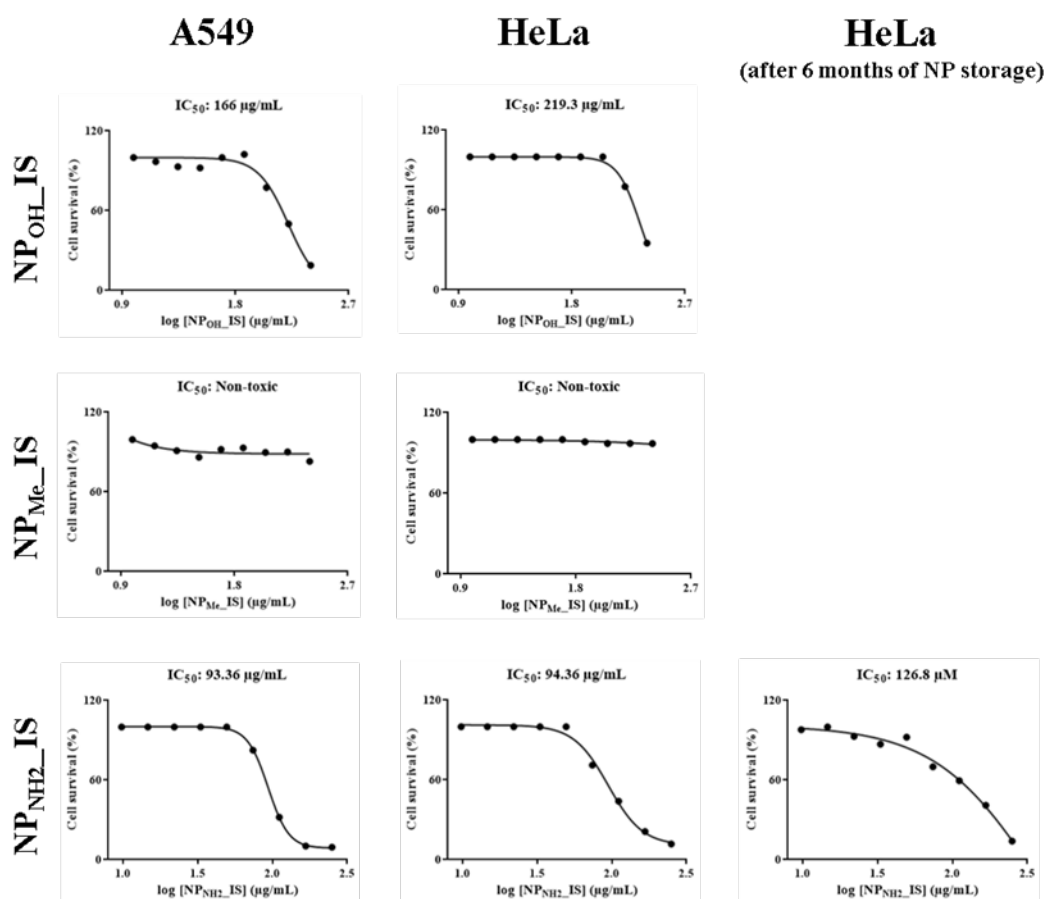


**Figure S15.** Dose-response curves for determination of the IC<sub>50</sub> cytotoxicity values of *in-situ* nanoparticles (NP<sub>OH\_IS</sub>, NP<sub>Me\_IS</sub>, NP<sub>NH2\_IS</sub>) in A549 (left column) and HeLa (central column) cell lines. NP<sub>NH2\_IS</sub> nanoparticles were tested again in HeLa cells after six months of storage in complete cell culture medium (right column). The IC<sub>50</sub> values correspond to the dose required to inhibit 50% cellular growth after cellular exposure to compounds for 72 h.

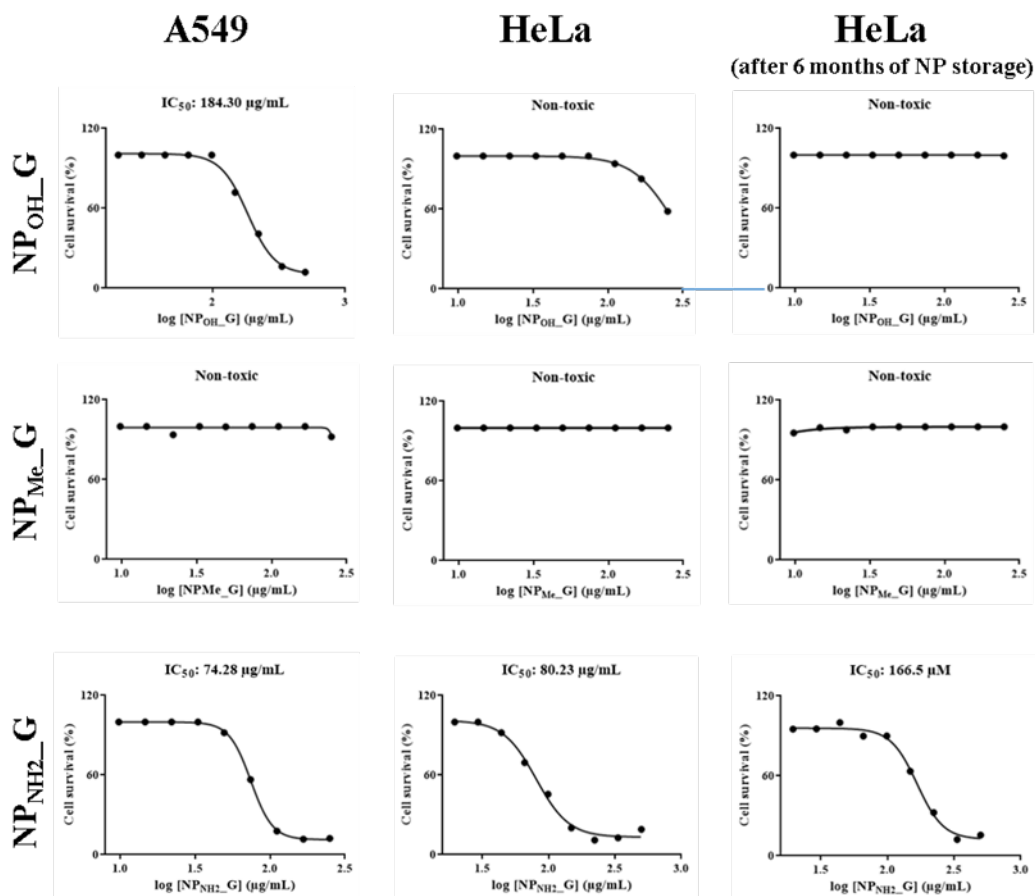


**Figure S16.** Dose-response curves for determination of the IC<sub>50</sub> cytotoxicity values of grafted nanoparticles (NP<sub>OH</sub>\_G, NP<sub>Me</sub>\_G, NP<sub>NH2</sub>\_G) in A549 (left column) and HeLa (central column) cell lines. Nanoparticles were tested again in HeLa cells after six months of storage in complete cell culture medium (right column). The IC<sub>50</sub> values correspond to the dose required to inhibit 50% cellular growth after cellular exposure to compounds for 72 h.

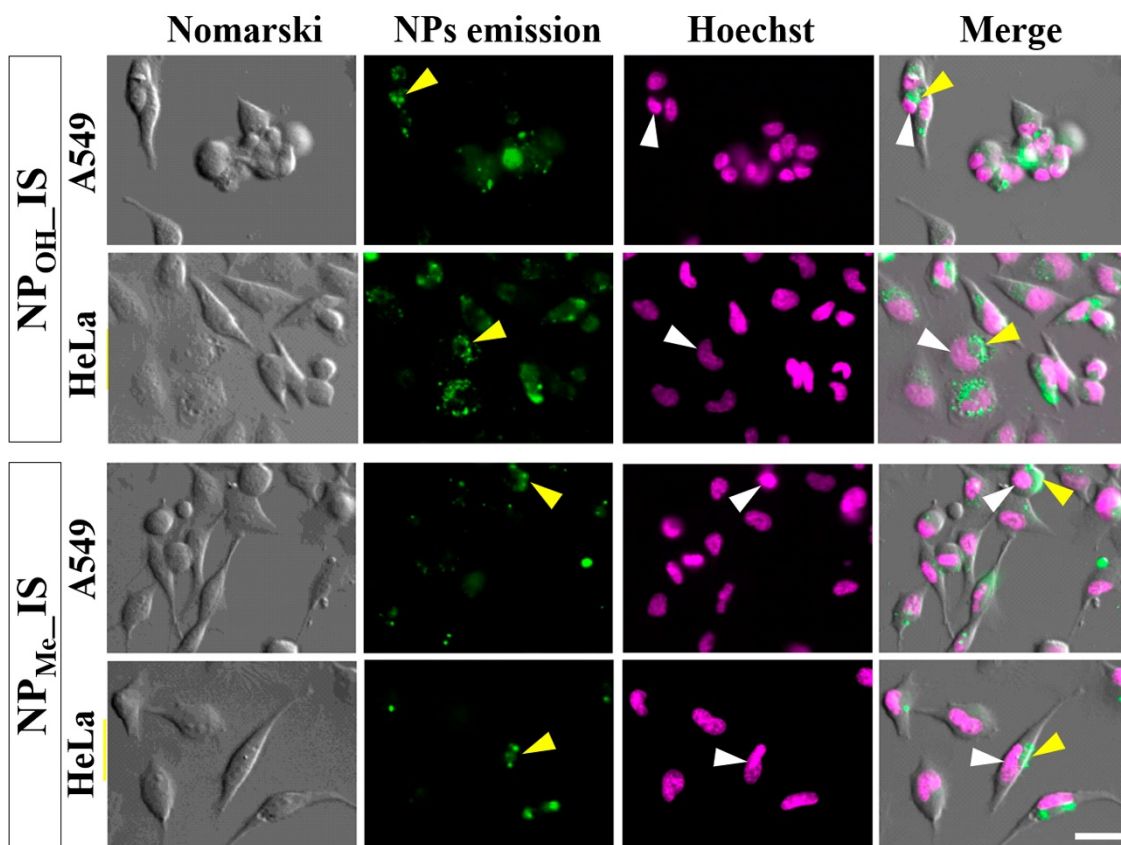


**Figure S17.** Fluorescence images of A549 and HeLa cells treated with *in-situ* nanoparticles NP<sub>OH-IS</sub> and NP<sub>Me-IS</sub>. Living cells were incubated with NPs (50 mg/mL) o/n at 37°C. Following, DNA binder Hoechst 33258 (3.2 μM) was added to the medium for 1 h. Cells were visualized by microscopy either for Nomarski white-light transmission (left panel), or fluorescence emission in green (central-left panel) and magenta (central-right panel). Overlays of Nomarski, green (NPs emission) and magenta (pseudocolor for blue emission, Hoechst) images are shown in right panels (merge). Both nanoparticles showed a similar behavior in both cell lines, locating mainly accumulated in cytoplasmic perinuclear areas (yellow arrowheads) but they do not co-localize with nuclei (white arrowheads). Scale bar: 30 μm.

## References for S.I.

1. (a) Pritchard, V. E.; Rota Martir, D.; Zysman-Colman, E.; Hardie, M. J., Multimetallic and Mixed Environment Iridium(III) Complexes: A Modular Approach to Luminescence Tuning Using a Host Platform. *Chem. Eur. J.* **2017**, *23* (37), 8839-8849; (b) Marchi, E.; Locritani, M.; Baroncini, M.; Bergamini, G.; Sinisi, R.; Monari, M.; Botta, C.; Mróz, W.; Bandini, M.; Ceroni, P.; Balzani, V., Blue and highly emitting [Ir(IV)] complexes by an efficient photoreaction of yellow luminescent [Ir(III)] complexes. *J. Mater. Chem. C* **2014**, *2* (22), 4461-4467.
2. Greenway, G. M.; Greenwood, A.; Watts, P.; Wiles, C., Solid-supported chemiluminescence and electrogenerated chemiluminescence based on a tris(2,2'-bipyridyl)ruthenium(II) derivative. *Chem. Commun.* **2006**, 85-87.
3. Becke, A. D., Density-functional thermochemistry. III. The role of exact exchange. *J. Chem. Phys.* **1993**, *98*, 5648-5652.
4. Frisch, M. J.; Trucks, G. W.; Schlegel, H. B.; Scuseria, G. E.; Robb, M. A.; Cheeseman, J. R.; Scalmani, G.; Barone, V.; Mennucci, B.; Petersson, G. A.; Nakatsuji, H.; Caricato, M.; Li, X.; Hratchian, H. P.; Izmaylov, A. F.; Bloino, J.; Zheng, G.; Sonnenberg, J. L.; Hada, M.; Ehara, M.; Toyota, K.; Fukuda, R.; Hasegawa, J.; Ishida, M.; Nakajima, T.; Honda, Y.; Kitao, O.; Nakai, H.; Vreven, T.; Montgomery, J. A.; Peralta, J. E.; Ogliaro, F.; Bearpark, M.; Heyd, J. J.; Brothers, E.; Kudin, K. N.; Staroverov, V. N.; Kobayashi, R.; Normand, J.; Raghavachari, K.; Rendell, A.; Burant, J. C.; Iyengar, S. S.; Tomasi, J.; Cossi, M.; Rega, N.; Millam, J. M.; Klene, M.; Knox, J. E.; Cross, J. B.; Bakken, V.; Adamo, C.; Jaramillo, J.; Gomperts, R.; Stratmann, R. E.; Yazyev, O.; Austin, A. J.; Cammi, R.; Pomelli, C.; Ochterski, J. W.; Martin, R. L.; Morokuma, K.; Zakrzewski, V. G.; Voth, G. A.; Salvador, P.; Dannenberg, J. J.; Dapprich, S.; Daniels, A. D.; Farkas; Foresman, J. B.; Ortiz, J. V.; Cioslowski, J.; Fox, D. J., *Gaussian 09, Revision B.01*. Gaussian, Inc., Wallingford CT, , 2010.
5. (a) Lee, C.; Yang, W.; Parr, R. G., Development of the Colle-Salvetti correlation-energy formula into a functional of the electron density. *Phys. Rev. B* **1988**, *37*, 785-789; (b) Becke, A. D., Density-functional exchange-energy approximation with correct asymptotic behavior. *Phys. Rev. A* **1988**, *38*, 3098-3100.
6. Barone, V.; Cossi, M., Quantum calculation of molecular energies and energy gradients in solution by a conductor solvent model. *J. Phys. Chem. A* **1998**, *102*, 1995-2001.
7. O'Boyle, N. M.; Tenderholt, A. L.; Langner, K. M., cclib: A library for package-independent computational chemistry algorithms. *J. Comput. Chem.* **2008**, *29*, 839-845.
8. (a) Martínez-Junquera, M.; Lalinde, E.; Moreno, M. T.; Alfaro-Arnedo, E.; López, I. P.; Larráyo, I. M.; Pichel, J. G., Luminescent cyclometalated platinum(II) complexes with acyclic diaminocarbene ligands: structural, photophysical and biological properties. *Dalton Trans.* **2021**, *50* (13), 4539-4554; (b) Millán, G.; Giménez, N.; Lara, R.; Berenguer, J. R.; Moreno, M. T.; Lalinde, E.; Alfaro-Arnedo, E.; López, I. P.; Piñeiro-Hermida, S.; Pichel, J. G., Luminescent Cycloplatinated Complexes with Biologically Relevant Phosphine Ligands: Optical and Cytotoxic Properties. *Inorg. Chem.* **2019**, *58* (2), 1657-1673; (c) Lalinde, E.; Lara, R.; López, I. P.; Moreno, M. T.; Alfaro-Arnedo, E.; Pichel, J. G.; Piñeiro-Hermida, S., Benzothiazole-Based Cycloplatinated Chromophores: Synthetic, Optical, and Biological Studies. *Chem Eur. J.* **2018**, *24* (10), 2440-2456.
9. Berenguer, J. R.; Pichel, J. G.; Gimenez, N.; Lalinde, E.; Moreno, M. T.; Pineiro-Hermida, S., Luminescent pentafluorophenyl-cycloplatinated complexes: synthesis, characterization, photophysics, cytotoxicity and cellular imaging. *Dalton Trans.* **2015**, *44*, 18839-18855.
10. Edelstein, A.; Amodaj, N.; Hoover, K.; Vale, R.; Stuurman, N., Computer Control of Microscopes Using µManager. *Current Protocols in Molecular Biology* **2010**, *92* (1), 14.20.1-14.20.17.
11. Lara, R.; Millán, G.; Moreno, M. T.; Lalinde, E.; Alfaro-Arnedo, E.; López, I. P.; Larráyo, I. M.; Pichel, J. G., Investigation on Optical and Biological Properties of 2-(4-

Dimethylaminophenyl)benzothiazole Based Cycloplatinated Complexes. *Chem Eur. J.*, <https://doi.org/10.1002/chem.202102737>.

12. OECD. 2010. Guidance Document on using Cytotoxicity Tests to Estimate Starting Doses for Acute Oral Systemic Toxicity Tests. No. 129. Paris, France. Available at: <https://www.oecd.org/chemicalsafety/testing/>.